J. Fluid Mech. (1999), *vol.* 382, *pp.* 1–26. Printed in the United Kingdom

Statistical analysis of local turbulent energy fluctuations

By G. GUJ AND R. CAMUSSI

Università di Roma Tre, Dipartimento di Ingegneria Meccanica ed Industriale,
via della Vasca Navale 79, 00146 Roma, Italy

(Received 3 June 1997 and in revised form 1 July 1998)

Time–frequency energy fluctuations of turbulent experimental velocity signals for $Re_\lambda \simeq 10$ and 800, are analysed using orthogonal wavelet transform. Some statistical properties of the energy bursts are analysed and discussed. The probability distribution functions (PDFs) of the energy amplitude fluctuations are investigated at different scales. Such PDFs show that the so-called non-intermittent and intermittent regions are characterized by quite different behaviour. Analysis of the wavelet coefficient scaling relations, averaged under suitable conditioning, reveals that the most energetic events localized in time and scale are responsible for the structure function (or wavelet coefficients) scaling anomalies related to intermittency. It is shown that the statistical properties which are correlated with the mechanism of the energy cascade from large to small scales are characterized by a universal behaviour. On the other hand, when the chosen statistical indicators are related to the characteristic size of turbulent structures, no universality is achieved, and a strong dependence upon the turbulent generator and Re_λ is observed. This is demonstrated by analysis of the statistics of time delays between successive events which show non-universal PDFs. The mean delay between successive intermittent events is also Re_λ dependent and increases for increasing Re_λ.

1. Introduction

The study of homogeneous and isotropic turbulence has usually been based upon two approaches which, sometimes, have yielded contrasting results. One is based on a statistical viewpoint that may be suitable for turbulence modelling, the other is based on direct analysis and superposition of basic vortical structures and is motivated by the importance that coherent structures have for drag reduction and flow control problems.

The statistical approach deals with the analysis of the velocity associated with a certain scale r or, equivalently, with the study of the p-order velocity structure functions, hereafter indicated by S_p, and defined as

$$S_p(r) = \langle |V_r|^p \rangle.$$

The symbol $\langle . \rangle$ denotes ensemble averaging over different realizations of the velocity difference $V_r = V(x + r) - V(x)$ whereas the absolute value is usually adopted to improve the statistical accuracy (see e.g. Camussi *et al.* 1996*a*). The main challenge of this statistical approach, based on the 1941 Kolmogorov theory (Kolmogorov 1941) and successively developed in many so-called *phenomenological* models (see e.g. the overview by Meneveau & Sreenivasan 1991), is the determination of universal

properties (always in a statistical sense) which account for the intermittent nature of the turbulent energy dissipation ϵ, and which are not dependent on the turbulence generator (see also Frisch 1996, for a general review).

Neither this approach nor the other based on the superposition of elementary structures (see e.g. Pullin & Saffman 1992; Lundgren 1982, 1993; Moffat 1984) is completely satisfactory mainly because of the lack of a direct and clear connection with the Navier–Stokes dynamics.

The most recent theoretical studies of homogeneous and isotropic turbulence attempt to correlate the universal properties observed in the velocity difference statistics with the presence and suitable combination of turbulent structures characterized by strong spatio-temporal coherence (see the statistical model proposed recently by She & Levesque 1994 and She & Waymire 1995). The meeting point between the two approaches may be found in the intermittent nature of the turbulent energy dissipation. It has in fact been demonstrated that intermittency, which in the present context refers to the non-Gaussian spatio-temporal distribution of the velocity gradients or of the rate of turbulent energy dissipation, is related to the presence of vortical structures with small characteristic size or of high vorticity, originated from the large-scale structures by the well-known stretching and folding process (Tennekes & Lumley 1972). The shape of such structures has been checked in numerical analysis of homogeneous and isotropic turbulence at moderate Reynolds numbers, to be filament-like (e.g. She, Jackson & Orszag 1990; Vincent & Meneguzzi 1991; Jimenez *et al.* 1993; Verzicco, Jimenez & Orlandi 1996) with a transverse size of the order of a few dissipative lengths $\eta = \nu^{3/4}\epsilon^{-1/4}$ where ν denotes the kinematic viscosity. These numerical results are also supported by some experimental studies (e.g. Kuo & Corrsin 1972; Douady, Couder & Brachet 1991; Villermaux, Sixon & Gagne 1995). Nevertheless, it appears that an appropriate and complete analysis of the statistical properties of such structures, as far as we know, has not yet been accurately performed.

An optimal tool for the analysis of spatio-temporal intermittent phenomena is the wavelet decomposition that, unlike the usual Fourier representation, permits the isolation of localized events both in time and frequency (or space and scale if, as in the present case, the Taylor hypothesis is adopted to exchange time and space). A complete review of the properties and advantages of the wavelet representation can be found in, among others, Farge (1992), Meneveau (1991) and Daubechies (1988). In a previous work, the present authors (Camussi & Guj 1997) have shown by means of a suitable wavelet-based identification technique that the properly normalized energy bursts at a selected scale r are directly correlated to the passage of coherent structures. Furthermore, they found that in different turbulence generators (namely, grids or jets) structures of different shapes are observed in spite of the universal statistics of the velocity structure functions. These results are the basis and the principal motivations of the present study.

In this paper, we present an analysis of the statistical properties of the energy bursts detected at different scales that, as already pointed out, are assumed to be induced by the passage of the coherent structures which animate the turbulent flow. Due to the connection between coherent structures and energy peaks at localized scales, the statistical properties of the energy fluctuations give direct information on the statistics of coherent structures, their temporal dynamics and their time-scale evolution. In our opinion these are fundamental aspects for understanding the role of coherent structures in real turbulence and their connection with the statistical laws of the velocity structure functions $S_p(r)$. Furthermore, in the present work we observe that some statistical properties of the energy fluctuations may show universal

behaviour in the sense that they seem not to be dependent on the turbulence generator or on Re_λ, which is the turbulent Reynolds number based on the Taylor microscale λ and the velocity r.m.s. On the other hand, when the statistical indicators are more directly correlated to the characteristic size and shape of coherent structures, different results are obtained for different flow configurations.

These observations are achieved by considering two experimental test cases which are characterized by quite different Re_λ and different turbulence generators. Specifically, we consider grid turbulence in isotropic and homogeneous conditions at very low Re_λ (~ 10) and locally homogeneous jet turbulence at high Re_λ (~ 800). The two test flow conditions both correspond to locally homogeneous and unbounded turbulent flows and only the longitudinal velocity component is measured in both cases. The measurement of only one velocity component of course represents a limitation of the present analysis. Nevertheless, the use of multiprobes or a numerical simulation would place limitations on the spatial resolution and on the maximum obtainable Re_λ. Furthermore, as demonstrated in Camussi & Guj (1997), the different turbulent generators considered here lead to quite different time signatures of the most energetic coherent structures correlated to the local energy fluctuations. Moreover, in that paper the authors have shown that the strongest differences were observed only on the longitudinal velocity component (the one parallel to the mean advection velocity). Therefore, the analysis of only the longitudinal velocity at the two Reynolds number considered is a meaningful quantity for the present purposes. The main aspect that we would like to clarify in this paper is the relation between the different type of structures originated by the different turbulence generators and the universality of the intermittency anomalies usually observed in locally homogeneous flows (most of the experimental analyses on this topic available in the literature are indeed based on grid or jet turbulence, see e.g. Arneodo *et al.* 1996). Indeed, part of this paper is devoted to showing that such different structures are responsible for the intermittency anomalies which are confirmed to be universal. On the other hand it is also shown that other statistical indicators, which are more directly correlated to the size and shape of the structures, are not universal. We consider that the characterization of the statistical properties of the energy bursts may contribute to the comprehension of the connection between the dynamics of vortical coherent structures and the statistical properties of homogeneous isotropic turbulence. This challenge may also be achieved by defining the limits of the observed statistical universality which, sometimes, hides the actual nature of turbulence.

The paper is organized as follows: in § 2 we present the methodology we have followed to determine the local energy fluctuations. The statistical indicators that we have chosen for the characterization of such energy fluctuations are presented in § 3. In § 4 experimental flow conditions are summarized and results are discussed in § 5. In § 6 final remarks and conclusions are presented.

2. Local energy fluctuations

The experimental velocity signals obtained through single-probe hot-wire measurements are processed by means of the orthogonal wavelet decomposition. Orthonormal wavelets of Battle–Lemarie type are used to decompose the velocity signals into a time–frequency (or space-scale) distribution of wavelet coefficients. None of the results achieved in the present work depend upon the wavelet type. Indeed, in the present analysis, wavelet decomposition is applied for the individuation of localized energy bursts and it has been checked that different types of wavelet kernel lead to energy

distributions whose largest peaks are localized at the same instants (see also Camussi & Guj 1997). We point out also that orthonormality ensures the invertibility condition and a limited (since non-redundant) number of coefficients to be analysed in the post-processing procedure. Details of the procedure adopted for the wavelet expansion can be found in Meneveau (1991) and Camussi & Guj (1997). Hereafter, $w(r, x)$ denotes the discrete wavelet coefficients obtained by the projection of the measured longitudinal velocity component, and corresponding to the scale r and at a time x, where neither r nor x are continuous functions. Specifically, the discretization of x follows from the frequency sampling adopted in the signal acquisition whereas the number of scales r is dependent on the length of the signal window over which the wavelet transformation is performed. In the present case, when segmentation of the signal was needed, we considered windows of 4096 samples, corresponding, in terms of space, to length scales much larger than the integral length, and leading to 12 scales (or resolution levels). The larger resolution always corresponds to a few Kolmogorov lengths η ($\sim 5\eta$).

As pointed out by Camussi & Guj (1997), the presence of turbulent structures, their singular shape and their temporal intermittent distribution lead to a non-uniform distribution of energy at the different scales r. The energy contained at a scale r and instant x can be simply evaluated as the square of the corresponding wavelet coefficient (see Meneveau 1991). However, a more suitable method of representing energy and intermittency in non-dimensional form at each selected resolution, can be achieved by the use of the so-called local intermittency measure (LIM, see Farge 1992) that is defined as

$$l(r, x) = \frac{w(r, x)^2}{\langle w(r, x)^2 \rangle_x}. \tag{2.1}$$

The averaging procedure, represented by the symbol $\langle . \rangle_x$, is performed by summing the normalized squares of the wavelet coefficients calculated at fixed scale r over the locations x and dividing by the number of instants (x). The two-dimensional function $l(r, x)$ represents the energy of the signal at a scale r and instant (or space location) x normalized by the total amount of energy contained in the signal at the scale r. For fixed $r = \bar{r}$, the spatial (or temporal) distribution of $l(\bar{r}, x)$ shows clear intermittent behaviour (examples are reported in Meneveau 1991; Farge 1992; Camussi & Guj 1997). This is more evident at larger resolutions, i.e. at smaller scales. The idea underlying the present analysis is that the peaks in the $l(r, x)$ distribution are induced by coherent structures which are passing close to the measuring probe location. The intermittent nature of $l(r, x)$ indicates the possibility that structures of different energy are characterized by a random phase whereas the different magnitudes of the $l(r, x)$ peaks suggests that the energy associated with the structures is also a random variable. In order to select structures of different energy, we can consider a scale $\bar{r}$ and choose a suitable threshold level t to be associated with the $l(r, x)$ distribution. In this way, we separate the wavelet coefficients into two sets: those corresponding to $l(\bar{r}, x) \geqslant t$ and, obviously, others for which $l(\bar{r}, x) < t$. An example of the $l(\bar{r}, x)$ distribution, is reported in figure 1. This case refers to a scale $\bar{r}$ of the order of few Kolmogorov lengths η and at $Re_\lambda \simeq 800$. In the framework of the present interpretation of the $l(r, x)$ distribution, the largest peaks of figure 1 are presumed to be induced by the passage of coherent structures. In the example of figure 1, we have fixed a threshold $t = 60$. If we consider $l(\bar{r}, x) \geqslant t$, we capture four events corresponding to the largest peaks. On the other hand, for decreasing t, a much larger number of events is detected. This event selection is the basis of the identification technique previously

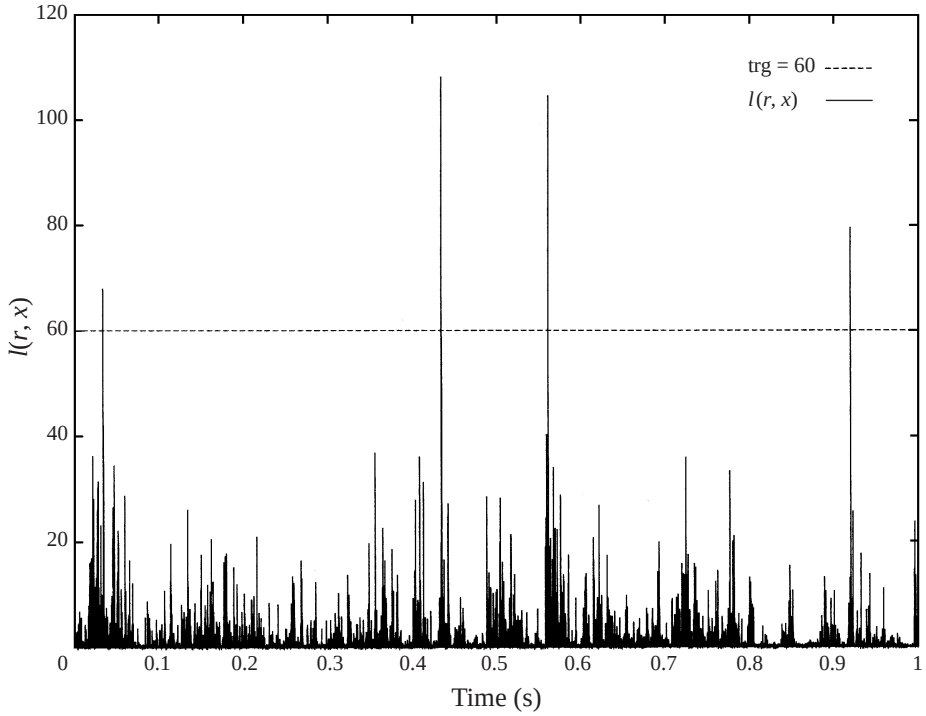

FIGURE 1. Example of a $l(r, x)$ distribution for $r \simeq 5\eta$ at $Re_\lambda \simeq 800$. A reference trigger level is shown at $t_1 = 60$ (dashed line) which leads to the selection of four events with $l(r, x) \geqslant 60$.

proposed by the authors (Camussi & Guj 1997). The selection of high or low energetic wavelet coefficients may be interpreted as a separation between coherent structures of high energy, and background turbulence which may also contain coherent structures with an energy distribution intermittent in phase, but with a lower degree of energy magnitude. As will be shown later, the independence of the presented results from the level of the threshold t indicates that physically there is no separation between coherent structures and background Gaussian turbulence. Therefore, we believe that, in view of the independence of the present analysis of the trigger threshold, the results obtained are not a consequence of an artificial separation between large and small energy fluctuations.

3. Energy burst amplitude and phase statistics

Several statistical indicators may be chosen for a general characterization of the turbulent energy fluctuations. The present work does not pretend to be exhaustive in this regard. Therefore, we try to consider some examples which are presumed to be representative of the energy fluctuation statistics and, thus, of the dynamical behaviour of coherent structures. More specifically, we are going to consider two principal classes of indicators which, as pointed out later, may lead to different interpretations. The first one refers to those quantities which are representative of the temporal dynamics of coherent structures and of the evolution of energy at different scales. We shall show that these parameters have almost universal properties. Indicators belonging to the second class are instead more directly dependent on the characteristic size and

shape of the turbulent structures. In this case no universality is achieved and a strong dependence upon the Re_λ and/or flow conditions is observed.

The principal indicators we have considered for a suitable statistical characterization of the turbulent energy fluctuations, are summarized in the following:

(*a*) *Probability distribution functions* (*PDF*) *of* $l(r, x)$: for each scale r we determine the PDF of $l(r, x)$ and compare such distributions for different scales and different flow conditions. In this case, the use of a threshold on $l(r, x)$ is adopted only to achieve better reliability of the PDF but, physically, the event selection is irrelevant. It is shown that there is a connection between the PDF of $l(r, x)$ and the shape of the energy spectra. The results obtained and some possible interpretations are given in § 5.

(*b*) *Scaling laws of the wavelet coefficients*: as verified in several works (Bacry *et al.* 1989; Farge 1992; Mimouni *et al.* 1995; Camussi & Guj 1997), when dealing with singular functions at a scale r, the wavelet coefficients and the velocity difference V_r scale in the same way. From the definition of $l(r, x)$ the following relation applies:

$$\text{if } V_r \propto r^\alpha \Rightarrow l(r, x)^{1/2} \propto |V_r|, \tag{3.1}$$

where α is a positive constant indicating that V_r is a continuous Holder function of order α. We can therefore introduce a new non-dimensional variable defined in the following way:

$$V_r^* = l(r, x)^{1/2}, \tag{3.2}$$

that, in view of (3.1), is representative of the velocity difference V_r. This quantity will be used later when dealing with the energy PDFs introduced in (*a*).

The scaling laws relative to the wavelet coefficients may be formalized as follows:

$$\langle w(r, x)^p \rangle_x = r^{\zeta(p)} \quad \text{or} \quad \langle |w(r, x)|^p \rangle_x = \langle |w(r, x)|^q \rangle_x^{\zeta(p)/\zeta(q)}. \tag{3.3}$$

The averages of this equation are performed by considering different realizations which correspond to the time instants x extending over the segments of 4096 samples, into which the whole signal has been divided. The right-hand side of (3.3) represents the application of the so-called extended self similarity (ESS) form of scaling (see e.g. Benzi *et al.* 1993; Benzi, Ciliberto & Chavarria 1995; Arneodo *et al.* 1996). This is a necessary tool for the determination of scaling exponents in moderate and low Reynolds number flows (see also Camussi *et al.* 1996*b*). The scaling exponents $\zeta(p)$ retain the non-Gaussian distribution of the turbulent energy dissipation since $\zeta(p) \neq p/3$ for $p \neq 3$ in contrast with the Kolmogorov prediction $\zeta(p) = p/3$ (see e.g. Frisch 1996). This is one of the better established results in the statistical analysis of homogeneous and isotropic turbulence and is supported by many experimental studies (see, among many, Anselmet *et al.* 1984). When, in (3.3), we consider $q = 3$, the left-hand side and right-hand side are equivalent since (Monin & Yaglom 1975):

$$\langle w(r, x)^3 \rangle_x \propto r \rightarrow \zeta(3) = 1. \tag{3.4}$$

In (Camussi & Guj 1997) we have shown that when only wavelet coefficients corresponding to $l(x, r) \geqslant t$ are retained, the $\zeta(p)$ obtained are, within the experimental uncertainty, the same as those resulting from the whole signal and are almost independent of Re_λ (for about $Re_\lambda \geqslant 10$) and the turbulence generator used. This result is extended and further checked in the present work by analysing two aspects. The first deals with the scaling properties of the properly smoothed wavelet coefficients. This analysis is performed by filtering out the wavelet coefficients corresponding to events $l(x, r) \geqslant t$. This means that, for different t, the coefficients selected are substituted

by linear interpolation between the previous (in terms of x and at the same r) and the subsequent coefficient (see also Abry *et al.* 1994). More specifically, when an event corresponding to $l(x, r) \geqslant t$ is detected at a scale $r = \bar{r}$ and for $x = x_0$, the interpolation procedure is performed for all scales at the same $x = x_0$. In this way the energetic contribution of the selected event is filtered out in the whole range of available resolutions. The application of ESS is therefore formalized as follows:

$$\langle |\tilde{w}(r, x)|^p \rangle_x = \langle |\tilde{w}(r, x)|^q \rangle_x^{\zeta(p)/\zeta(q)}, \tag{3.5}$$

where $\tilde{w}(r, x)$ represents the set of wavelet coefficients properly smoothed each time the corresponding $l(x, r)$ overcame the threshold. Therefore, even if the averages are still performed upon all x as in (3.3), the wavelet decomposition is necessary in order that proper smoothing at selected instants be performed.

The second aspect is the analysis of the scaling properties of the wavelet coefficients corresponding to $l(x, r) < t$ for different t. In this second approach, we consider the following scaling relation:

$$\langle |w(r, x_0)|^p \rangle_{x_0^t} \sim \langle |w(r, x_0)|^3 \rangle_{x_0^t}^{\zeta(p)}. \tag{3.6}$$

This conditional average is therefore performed only over the wavelet coefficients at the instants x_0^t that correspond to $l(r, x_0) \leqslant t$. It is expected that the lower t the lower should be the intermittency anomaly and the Kolmogorov $p/3$ scaling should be achieved asymptotically for decreasing t. Also in this case, the proper selection of the instants x_0^t may be performed only by taking advantage of the locality in time of the wavelet coefficients, and could have not been achieved by a simple Fourier transform.

The question that we would like to clarify with the analysis of such scaling relations, is whether the energy fluctuations are representative of the intermittent behaviour usually observed in the velocity structure functions. Furthermore we would like to analyse how the filtering or thresholding procedures affect the scaling exponents and whether they are dependent upon Re_λ or the turbulence generator. This corresponds to analysing what is the influence of the coherent structures on the structure function scaling laws and whether their effects are dependent on the way turbulence is generated. For further discussion and presentation of results, we again refer to § 5.

(*c*) *Waiting times*: following the procedure applied to pressure fluctuations by Abry *et al.* (1994), we analyse the PDF of the time delays between successive events in the anemometric signal. In this case, the only selected time instants x_0 are those corresponding to $l(r, x_0) \geqslant t$. This analysis is limited to scales r corresponding to a few Kolmogorov lengths in order to get sufficient reliability of the PDFs since, in view of the orthonormal wavelet expansion, the smaller the scale the larger the number of events detected. It is shown that such PDFs are strongly non-Gaussian. Furthermore, it is shown that the functional form of such distributions depends upon the flow conditions and that their shape may give an indication of the characteristic size of the most probable coherent structures. The different behaviour found in different flow conditions will be interpreted (in § 5) in terms of the effects of the different turbulent structures which characterize grid and jet turbulence and which affect the waiting time PDFs. The observed differences are then to be associated, as will be pointed out later, with a correlation length typical of the coherent structures which characterise the turbulent flow considered.

Finally, we also calculated the mean waiting time between successive events, that, properly normalized, again shows a strong dependence on Re_λ.

Case	$\bar{V}$ (m s^{-1})	σ_V (m s^{-1})	η (mm)	λ (mm)	Re_λ	$N_{tot} \times 10^6$	$F_s \times 10^3$ (s^{-1})
Grid	2.5	0.0290	~ 0.80	$\sim$6.3	~ 10	3	16
Jet	8.4	2.0310	~ 0.10	$\sim$7.0	~ 800	16	16

TABLE 1. Flow conditions and acquisition parameters of the two test cases considered: grid represents homogeneous grid turbulence at $x/M = 163$ (with M the mesh size); jet represents the experiment in fully developed jet turbulence at $x/D = 23$ (with D the jet diameter). $\bar{V}$ is the mean axial velocity at the measurement positions and σ_V is the standard deviation of the longitudinal velocity. N_{tot} is the total amount of acquired samples with frequency sampling F_s.

In conclusion, we point out that the indicators (*a*) and (*b*), in addition to other consequences which will be discussed later, are examples of statistical properties which show universality. On the other hand, the indicator (*c*) is representative of those which are affected by the different nature of coherent structures which seem to depend on the way turbulence is generated and on the Re_λ of the flow.

As pointed out above, all the adopted indicators are based on the locality in time (or space) of the wavelet coefficients and the consequent results that will be presented in § 5 could have not been obtained by projecting the signals over the Fourier modes.

4. Experimental data and measurement reliability

Experimental data are obtained from single-probe hot-wire measurements performed in grid and jet turbulence. Two very different test cases are considered, and the corresponding Re_λ differ by about two orders of magnitude (from ~ 10 to ~ 800, a value not attainable by numerical simulation). Flow conditions are summarized in table 1 for the grid and jet test cases. For details of the experimental arrangements and measurement techniques, see Camussi *et al.* (1996*a*), and Camussi & Guj (1996).

As already pointed out, the use of a single sensor probe has been dictated by requirements of spatial resolution and low intrusivity. This of course represents a limitation to the interpretation of the physics of the phenomenon and introduces an error (of the order of 4 % for a relative turbulence level of about 20 %) due to the second-order terms neglected in the Taylor expansion (Jorgensen 1971).

We should also point out that measurements at both very low and very high Re_λ may present further difficulties in ensuring good accuracy of the acquired data.

In the grid case, the main source of errors is correlated to the very low turbulence level of the flow and, therefore, to the possibility that the background noise (e.g. due to electronic and electro-magnetic effects, ground and probe vibrations and the A/D converter resolution) may reach the same order of magnitude as the velocity fluctuation amplitude. This aspect is significant when wavelet decomposition is performed, since the smaller the scale selected the smaller the expected signal-to-noise ratio. In order to avoid these problems the hot-wire signals have been treated with a procedure appropriate to a small fluctuating velocity. Specifically, the anemometric signal has been acquired with a suitable offset and amplification, and it has been split into the AC and DC components by an analogue filter. The AC signal alone has been further amplified (gain of 30 or larger) in order to approach the full scale of the 12 bit A/D converter used. After the acquisition, the mean and fluctuating components have been rescaled numerically, and finally recombined. It has been checked that this procedure ensures good reliability of data even at the smallest scales (for further details see Camussi & Guj 1996).

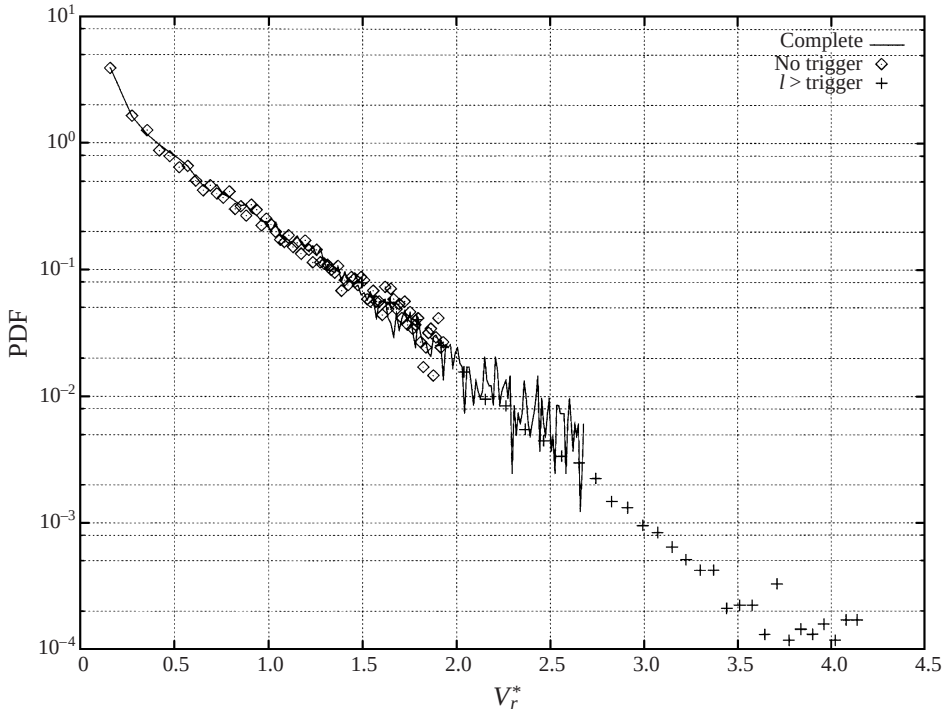

FIGURE 2. Log-linear plot of the PDFs of the $l(r, x)$ fluctuations computed for $r \simeq 5\eta$ and $Re_\lambda \simeq 10$. Solid line corresponds to the PDF using the whole signal. Symbols correspond to the PDF resulting from the methodology proposed in § 5.1. The PDF amplitudes are normalized to achieve a unitary integral.

At high Re_λ (the jet case), we consider the probe resolution filtering effects as the main possible cause for a lack of measurements accuracy. However, in this case, measurements have been performed using a micro-sensor (probe TSI 1260) of length $l_w = 500\,\mu\text{m}$, which ensures a resolution of the order of 5 Kolmogorov lengths (Camussi *et al.* 1996*a*). Also this aspect is important when dealing with the small scales achieved by wavelet decomposition which, therefore, has always been limited to $r \geqslant l_w$ (by analogy, also in the grid case analyses the smallest scale considered has been fixed to $r \simeq 5\eta$). We also point out that the relative turbulence level in the jet flow is on the order of 25 %. This value represents approximately the upper limit for correct application of the Taylor hypothesis (e.g. Monin & Yaglom 1975).

5. Results and discussion

In this section, principal results are presented and discussed. The three following subsections refer to the three indicators that, see § 3, have been chosen for statistical analysis. As pointed out above, the approach adopted in the present work is purely statistical, in the sense that the shape of coherent structures and their detailed topological features are not directly found. Nevertheless, we show that some of the indicators chosen may retain some of the topological properties of the coherent structures.

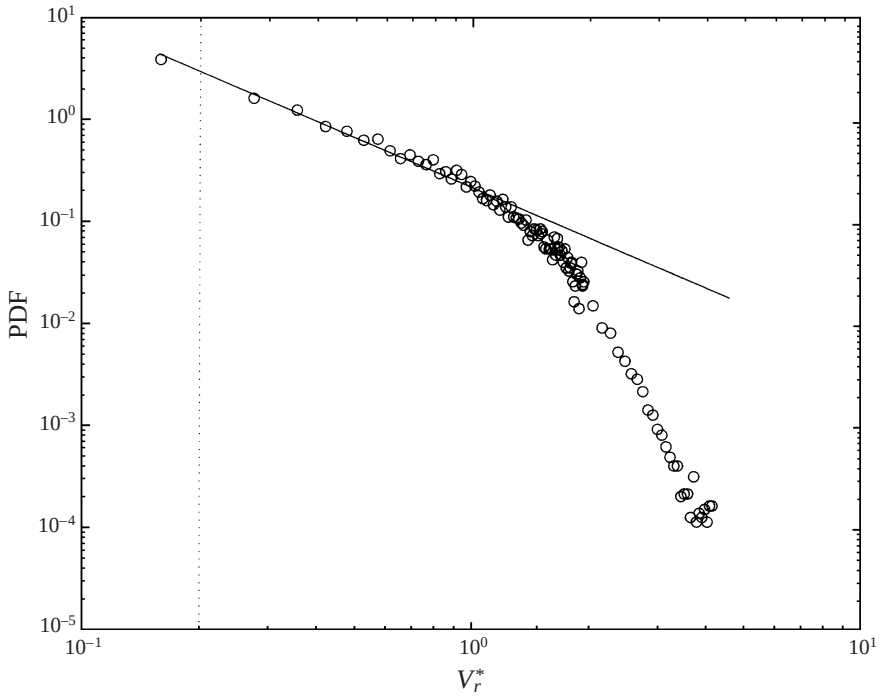

FIGURE 3. Same as on 2 but on a log-log scale. The solid straight line represents the fit computed for $V_r^* \leqslant 1$ which yields a slope $\simeq -1.62$. Points corresponding to $V_r^* \ll 1$ are not reported for clarity but the noise level corresponds to the vertical dotted line.

5.1. *PDF of local energy fluctuations*

First of all it should be pointed out that, in order for sufficient reliability of the PDF to be achieved at high energy levels (where the statistics is poor), a large number of samples, corresponding to the whole signal length (see N_{tot} in table 1), has to be considered. Therefore the determination of the PDF of $l(r,x)$ may require too much CPU time and disk space. Here we propose an alternative and more efficient procedure based on the thresholding technique previously described. In this method we consider different subranges of energy amplitudes to match the whole PDF of $l(r,x)$. First a short segment of points is considered (specifically on the order of 10^4 samples) where the wavelet decomposition is applied so that a reliable PDF for small fluctuations results due to the large number of events with low $l(r,x)$. Then, the whole signal is considered, and the PDF is computed only over those events with $l(r,x) \geqslant t_1$ where t_1 is a suitable trigger level; the procedure is repeated for various $t_i > t_1$ and the complete PDF may finally be obtained but using a number of samples much smaller than that corresponding to the whole signal length. Furthermore, it has been checked that the rare and intermittent events are better resolved than the direct analysis of the whole signal, due to the locality of the $l(r,x)$ definition (see (2.1)).

As a first test, we consider the grid case and analyse the $l(r,x)$ distribution for $r \simeq 5\eta$. We therefore refer to the small-scale energy fluctuations (not affected by noise or probe resolution errors) at $Re_\lambda \simeq 10$. In figure 2, a comparison of the PDF obtained with the proposed procedure and that considering the whole signal is shown on a linear-log scale. The two curves superimpose and that obtained with the new procedure shows a quite smooth behaviour and is much more extended in terms

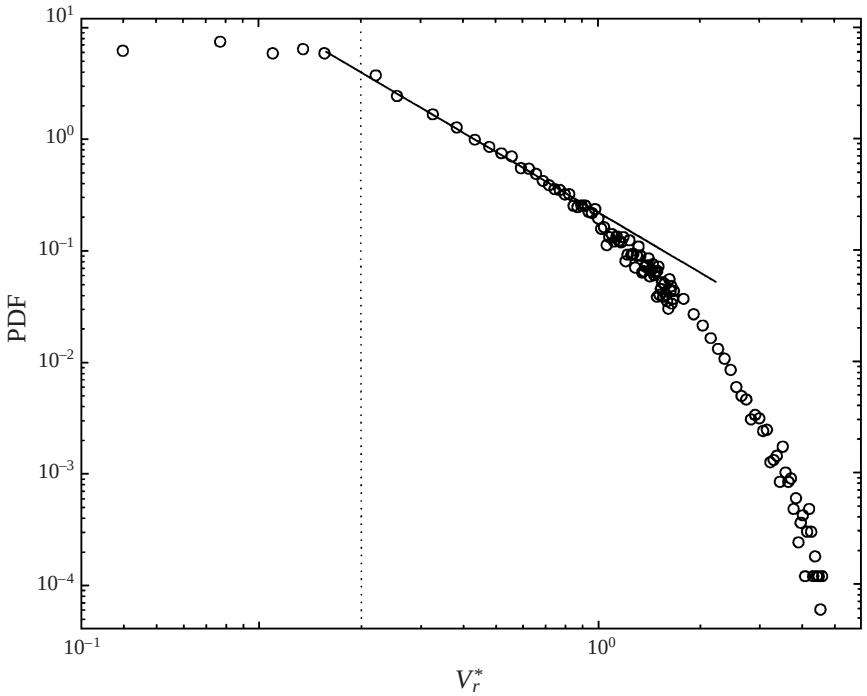

FIGURE 4. Same as figure 3 but for $Re_\lambda \simeq 800$. The solid straight line is obtained by the fit computed for $0.2 \leqslant V_r^* \leqslant 1$ and yields a slope $\simeq -1.7$. The points for $V_r^* \ll 1$ are also drawn and the flattening observed for about $V_r^* < 0.2$ corresponds to the effect of the Gaussian background noise (vertical dotted line).

of $l(r, x)$. The x-axis of figure 2 actually represents the non-dimensional variable V_r^* introduced in (3.2). The plot in figure 2 shows that the functional form of the PDF is close to exponential except for $V_r^* \leqslant 1$ whose functional behaviour will be discussed in the following. This result is in agreement with previous observations of the PDF of the velocity difference at small separation scales (see e.g. Castaing, Gagne & Hopfinger 1990). The same PDF is shown in figure 3 on a log-log scale. A power law in the region $0.2 \leqslant V_r^* \leqslant 1$ is exhibited with an exponent $\sim -1.62 \pm 0.07$. The vertical dotted line represents the noise level defined in detail in the following.

In figure 4, the PDF for the case of $Re_\lambda \simeq 800$ and at a scale also on the order of 5η is shown on a log-log scale. Three regions may be seen in this plot. The very small V_r^* range is useful for a definition of noise effects. Indeed, it is observed that for $V_r^* < 0.2$ the curve becomes flat indicating the prevalence of the Gaussian background noise over physical effects. The region $0.2 < V_r^* < 1$ corresponds to points where a power law applies. A linear fit (in the log-log representation) has been performed within this region yielding an exponent of $\sim -1.7 \pm 0.05$. The experimental uncertainty of the scaling exponent has been calculated by the standard deviation of the set of all the possible slopes achieved among the points in the selected range where the fit is performed (see Camussi *et al.* 1996*b*). A transition from a power to an exponential law is finally observed for about $V_r^* \simeq 1$ and it has been shown in a log-linear representation (not reported here for brevity) where a linear trend corresponds to the exponential decay.

In figure 5, the two PDFs, at $Re_\lambda \simeq 800$ and 10, are shown together, excluding points affected by the background noise. The collapse of the points is satisfactory,

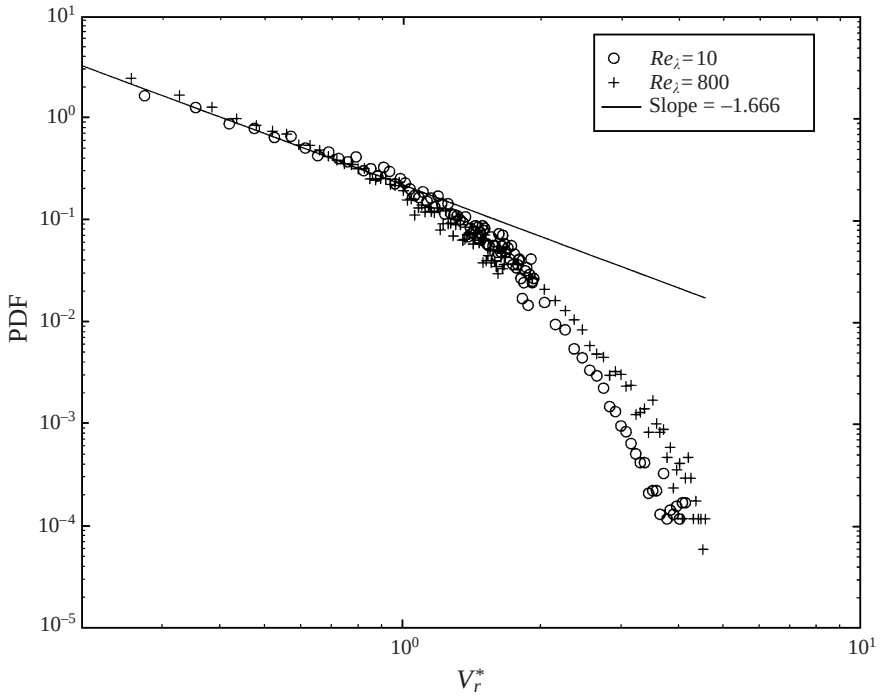

FIGURE 5. Superimposition, on a log-log scale, of the PDFs of figures 3 and 4 in the region not affected by background Gaussian noise ($V_r^* > 0.2$). Different symbols correspond to different Re_λ. The solid straight line is obtained by the fit computed for $0.2 \leqslant V_r^* \leqslant 1$ considering both Re_λ cases.

within the experimental uncertainty, except for very high V_r^*. For $0.2 < V_r^* < 1$ a power law behaviour is observed in both cases, and the superposition is achieved without any further normalization.

The same analysis is then applied to resolutions corresponding to larger scales, on the order of the integral length; the result obtained for $Re_\lambda \simeq 10$ is shown in figure 6 and compared with the small-scale PDF at the same Re_λ. It should be pointed out that, since larger scales are considered, a coarser decomposition is performed by the wavelet expansion, and a significantly lower number of events is detected with respect to the cases at small r. This explains the larger dispersion of the experimental points in figure 6, and causes such results to be only qualitatively valid. Taking this into account, it can be observed that the collapse of the curves corresponding to small and large scales is achieved anyway and that the fit leads to a slope close to the one previously obtained. Analogous behaviour is observed for $Re_\lambda \simeq 800$ (not reported here) even if for high Re_λ the separation between dissipative and integral scales is quite significant. The collapse of the curves for large scales is also obtained for the two Re_λ (figure 7), giving, in this case even though in a more qualitative manner, also a power law with an exponent again close to -1.65 ± 0.22. Note that in the cases of figures 6 and 7, we focus attention on the region where a power law applies and, therefore, the points corresponding to larger V_r^* are not drawn. Nevertheless, when the curves of figures 6 or 7 are plotted in a semi-log scale (not reported here for brevity) an exponential trend is again qualitatively observed for large V_r^*. Also, the region where these curves are affected by the background noise is not reported for clarity. With reference to figures 6 and 7 we can claim that universality seems

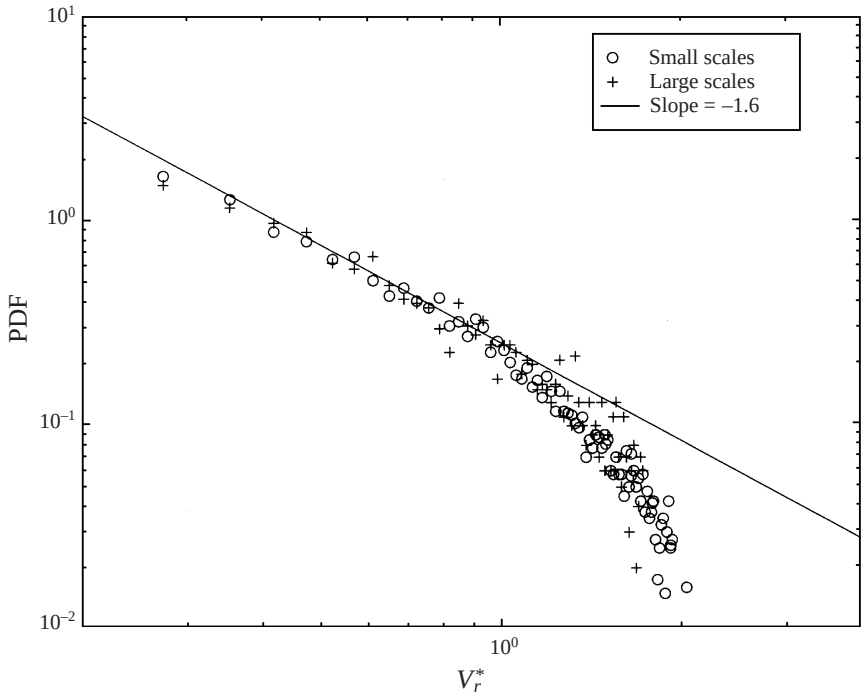

FIGURE 6. Log-log plot of the PDF at $r \simeq L_0$ (where L_0 denotes the integral length) compared with that obtained for $r \simeq 5\eta$. Both curves are calculated for $Re_\lambda \simeq 10$. The fit represented by the solid straight line is obtained considering both the small- and large-scale PDFs in the range $0.2 \leqslant V_r^* \leqslant 1$.

confirmed again for small V_r^* since, in this range, the observed shape of the PDFs is not dependent upon the scale selected and the flow conditions.

We can summarize what has been observed so far as follows: the PDFs of the $l(r, x)$ as functions of V_r^* are characterized by a power law at small V_r^* and an exponential law at larger V_r^*. The transition from a power to an exponential law is observed for $l(r, x) \simeq 1$. Such a functional form is achieved from the integral down to dissipative scales r where the $l(r, x)$ distribution is computed, and seems independent of Re_λ. Furthermore, the region where a power law applies, seems to be universal, in the sense that, without any normalization (apart from that adopted to get a unitary integral in the PDF distribution), all the curves collapse at small V_r^* independently of r and Re_λ. As pointed out above, the region where a power law applies corresponds to $l(x, r) \leqslant 1$ which can be considered the range of nonintermittent energy distribution (see Farge 1992).

An important result achieved in the PDF analysis is that not only is the PDF of the energy distribution non-Gaussian but, when intermittency is not considered (i.e. when $l(r, x) < 1$), its functional form becomes a power law. A naive correspondence between the PDF shape (see e.g. figure 3 and figure 4) and the energy spectra within the inertial range at high Re_λ may be argued and seems confirmed by the exponent of the power law region that incidentally is very close to $-5/3$. Nevertheless, as yet this behaviour has no physical and theoretical explanation (see also Yamada, Kida & Ohkitani 1993).

From a statistical viewpoint, the transition from a power law to an exponential law in the energy fluctuation PDFs can be attributed to the different nature of the events

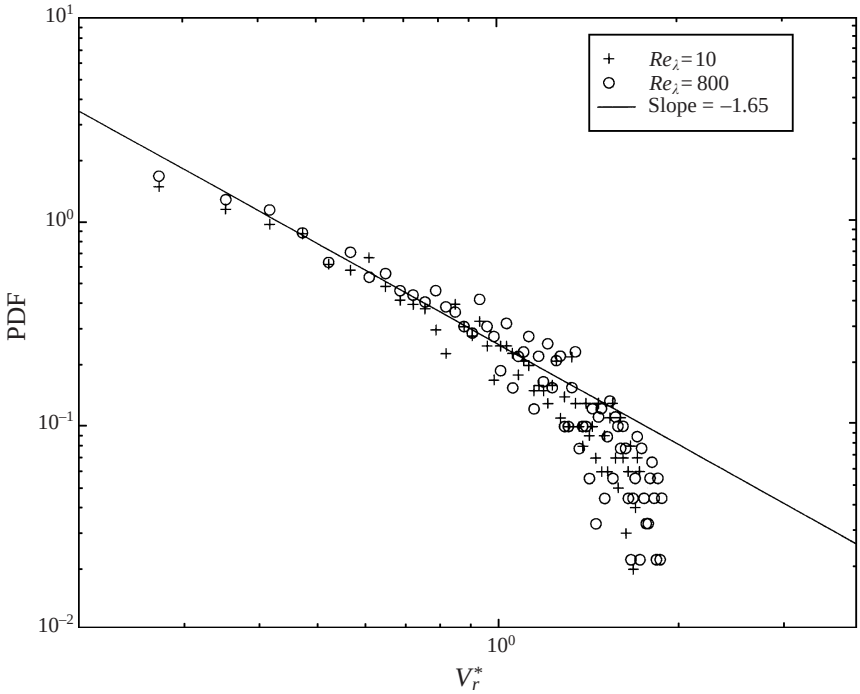

FIGURE 7. Log-log plot of the PDFs at $r \simeq L_0$ for the two flow conditions considered. Different symbols correspond to different Re_λ. The fit represented by the solid straight line is obtained considering both PDFs in the range $0.2 \leqslant V_r^* \leqslant 1$.

selected. A power law behaviour can be considered proper for self-similar random variables whereas exponential PDFs are proper for statistically independent variables (see Abry *et al.* 1994). It has been found that the transition from a power to an exponential law corresponds to the appearance of intermittency, that is for $l(r, x) \simeq 1$ (see Farge 1992). Therefore we may argue that, for a fixed scale r, there is a cascading process from high to low energy levels similar to what happens in the Fourier domain when going from large to small scales. Indeed, the largest energy fluctuations, as for the case of small scales when considering the Fourier domain, are characterized by an intermittent nature which is revealed, by analogy with the PDF of the velocity differences at small scales (Castaing *et al.* 1990), by the exponential PDF.

We recall that the PDFs presented so far are calculated at fixed scales r and by analysing the energy fluctuations in the time domain (apart from the Taylor hypothesis). It is therefore not clear whether the observed energy amplitude variations may be interpreted as induced on the scale r by structures of different energy, or, taking into account that the signals are achieved using a probe in a fixed position, whether the observed effects are due to structures passing at different distances from the probe. At any rate, the exponential decay of the energy fluctuation PDFs in the intermittent range seems to support the idea of a log-Poisson distribution of the energy dissipation fluctuations (see e.g. Dubrulle 1994). However, it seems beyond doubt that the $l(r, x)$ PDFs have universal behaviour independent of the possible physical mechanisms leading to their shapes. This is a non-trivial result if we account for the large differences in the flow conditions (Re_λ magnitudes and turbulence generators) and for the basic differences in the topological nature of the structures

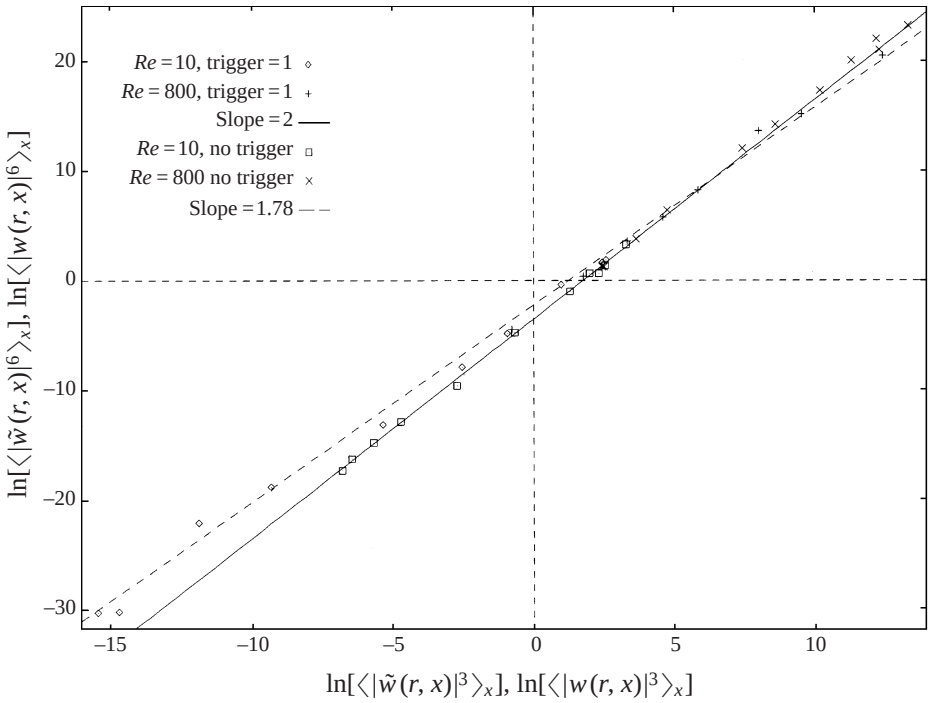

FIGURE 8. Scaling relation between wavelet coefficients obtained considering the smoothing procedure proposed in § 3. The points corresponding to scales $r < 5\eta$ are not shown and not considered in the fit. The slope $\simeq 2$ corresponds to a trigger threshold of about 1 ($\langle|\tilde{w}(r,x)|^p\rangle_x$) whereas the slope $\simeq 1.78$ corresponds to the fit performed over non-filtered coefficients ($\langle|w(r,x)|^p\rangle_x$). The scales are linear and the data are expressed in natural logarithms.

related to the $l(r,x)$ fluctuations in grid and jet turbulence (see Camussi & Guj 1997, where such large differences were demonstrated by the longitudinal velocity component analysis).

5.2. *Scaling laws and intermittency exponents*

When the wavelet coefficients corresponding to strongly peaked events in the $l(r,x)$ distribution are smoothed out by the linear interpolation explained in § 3, the degree of intermittency of the velocity signal decreases. In figure 8, the effects of the smoothing procedure are reported. The most interesting result is the elimination of the intermittency anomalies in the scaling exponents. In fact, for a threshold level equal to 1, a slope of 2 is found instead of the usual anomalous exponent (of about 1.78) expected for fully turbulent conditions (see e.g. Anselmet *et al.* 1984; Vincent & Meneguzzi 1991). The $\langle|\tilde{w}(r,x)|^p\rangle_x$ (with $p = 3$ and $q = 6$) used in figure 8 represents the wavelet coefficients averaged over the whole set of time instants after the smoothing procedure (3.5). The anomalous behaviour obtained with no smoothing of the wavelet coefficients, yielding the expected scaling 1.78, is also shown in the figure for comparison. Indeed, for the threshold level fixed at 1, almost all of the $l(r,x)$ fluctuations are eliminated. The consequent scaling is therefore closer to the Kolmogorov prediction and the relative scaling exponent $\zeta(6)/\zeta(3)$ is close to 2 with a difference of less than 5 %. Therefore, the physical interpretation of these results follows the expected idea that the smoothing procedure leads to the elimination

of the intermittent events with high energy and, when the energy spottiness is almost completely eliminated, the Kolmogorov prediction is consequently achieved (see e.g. Willaime *et al.* 1996).

Another important consequence of these results is that structures associated with the energy bursts observed on the $l(r, x)$ distribution, are the only events responsible for the observed intermittent behaviour of the velocity structure functions (that are directly represented by the averaged wavelet coefficients). Indeed, when such events are eliminated, intermittency anomalies are no longer observed. It should be pointed out that the fit is achieved considering both $Re_\lambda \simeq 10$ and $Re_\lambda \simeq 800$ and accounting for coefficients corresponding to $r \geqslant 5\eta$, in order to avoid probe resolution errors at very small scales (see § 4).

From the analysis of the energy spectra, it has also been checked that this scale is not affected by round-off errors. Moreover it can be observed that both in the smoothed and in the raw wavelet scalings, not only the scaling exponents but also the prefactors of the scaling laws are retained and are not dependent on the flow conditions considered. Finally, we want to focus also on the wide scaling ranges in figure 8. These extend over intervals of about 10 decades (the plot of figure 8 uses a natural logarithm). Such an extension is related to the large difference between the Re_λ of the two cases considered and supports the reliability of the scaling exponent estimation.

These results are achieved also for other moment orders ($p < 6$) which are not reported here for brevity.

In order for these results to be checked further, the scaling laws have been calculated again considering only those events with energy lower than the trigger threshold. In other words, instead of smoothing out the contribution of the wavelet coefficients corresponding to energy levels larger than the trigger threshold, such events are not accounted for in the averaging procedure for the computation of the scaling relations (see § 3). In this case, when the threshold level is high (that is, $t \gg 1$), the scaling exponents and intermittency anomalies usually observed, are achieved. On the other hand, when $t \simeq 1$, most of the peaked energy fluctuations are eliminated and the Kolmogorov scaling is again achieved. These results are shown in terms of scaling exponents in figure 9 (*a*). It is confirmed that intermittency is related only to the peaks of the $l(r, x)$ distribution since their elimination leads to the disappearance of the intermittency anomalies. An asymptotic trend is observed for $t \to 0$ which corresponds to $\zeta(6) \to 2 \pm 0.05$, whereas for $t \to \infty$ $\zeta(6) \to 1.75 \pm 0.04$. The points of figure 9 (*a*) are also reported in log-linear scales in figure 9 (*b*). The x-axis represents the root of the trigger level that, in view of (3.1), can again be represented as V_r^*. In a qualitative manner, it can be observed that the functional form is close to exponential and that the exponent achieved by a linear fit of the log-linear points is similar for the two Re_λ considered.

In summary it has been shown that, within the experimental uncertainty (on the order of 5 %), the scaling exponents are universal, and their transition towards a Kolmogorov scaling, achieved for decreasing t, also follows a functional form which does not vary for different flow conditions. Therefore, this approach also supports the idea that the way energy is distributed among different scales as a consequence of the cascading process, is universal and preserves the corresponding scaling relations of the velocity structure functions, independently of Re_λ. In summary the results of figure 8 and figure 9 (*a*, *b*) support the idea that coherent structures are responsible not only for the $l(r, x)$ fluctuations but also for the intermittency anomalies usually observed since, when the largest $l(r, x)$ fluctuations are not considered (by the smoothing procedure

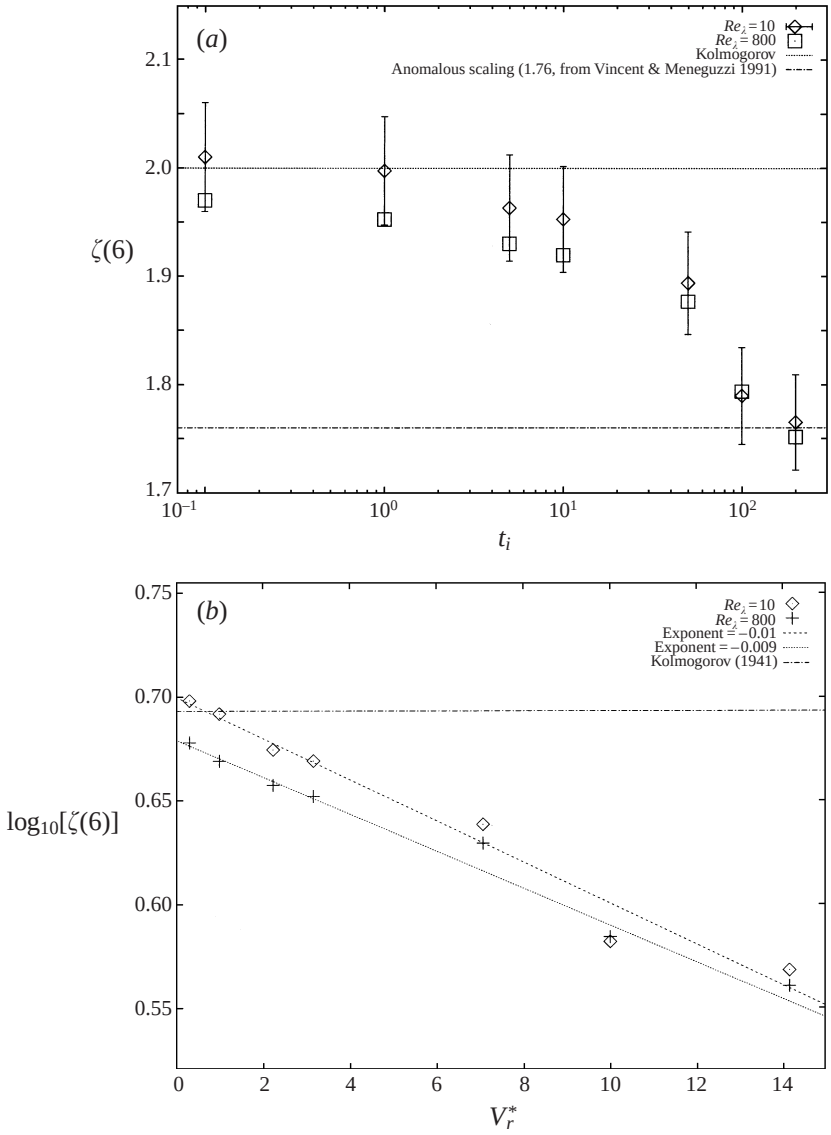

FIGURE 9 (a, b). Scaling exponents $\zeta(6)$ from (3.3) (using ESS) and for different trigger thresholds. (a) $\zeta(6)$ as a function of t_i. Different symbols correspond to different Re_λ and the error-bars are shown only for $Re_\lambda \simeq 10$. (b) Log-linear plot of $\zeta(6)$ as a function of $V_r^* = t_i^{1/2}$. A functional form close to exponential is achieved for both Re_λ and the exponents values are reported in the legend.

of figure 8 or by their direct elimination in figure 9 (a, b)) intermittency anomalies also disappear and the Kolmogorov scaling is observed.

Further analysis has been performed by considering the energy associated with the structures which are filtered or eliminated by the conditioning procedure described above. Specifically, E_s^r denotes the energy of the structures which are eliminated or smoothed at a scale r ($\simeq 5\eta$). On the other hand, E_s denotes the energy associated with structures which are eliminated or smoothed over all the scales r. The energy computation is performed in the wavelet domain and the definitions of the energy

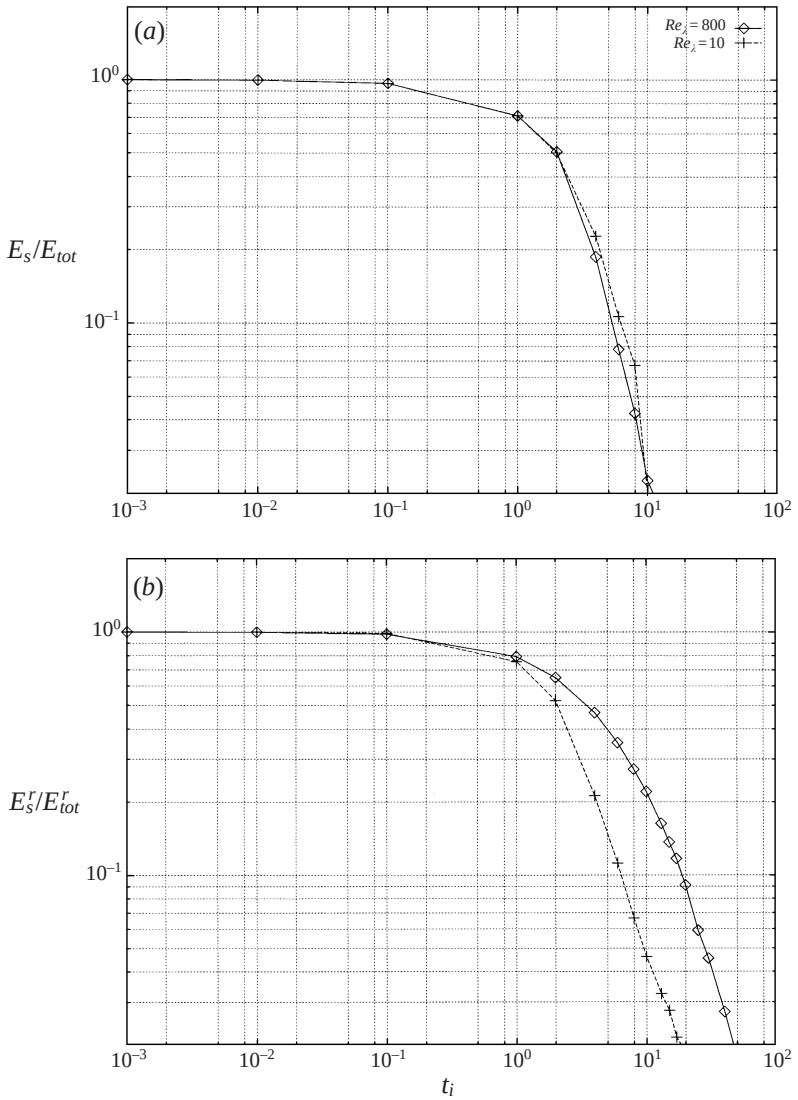

FIGURE 10 (a, b). Log-log plot of the energy ratios defined in (5.1) and (5.2), for the two test cases. (a) E_s/E_{tot}, (b) E_s^r/E_{tot}^r.

contents may be formalized as follows:

$$E_s^r = \sum_{x_0^t} w(r, x_0^t)^2 \quad \text{and} \quad E_s = \sum_{x_0^t} \sum_r w(r, x_0^t)^2. \tag{5.1}$$

The selection of the spatial positions x_0^t is performed as previously described, i.e. by fixing a level t and conditioning over the $l(r, x)$ distribution.

The question that we would like to clarify is how important is the contribution of the small-scale structures to the total energy of the turbulent flow. This point is analysed by considering the ratios E_s^r/E_{tot}^r and E_s/E_{tot} for different t_i where:

$$E_{tot}^r = \sum_x w(r, x)^2 \quad \text{and} \quad E_{tot} = \sum_x \sum_r w(r, x)^2. \tag{5.2}$$

Indeed, when $t_i \to 0$, it is expected that both ratios tend to 1 since almost all fluctuations are filtered whereas when $t_i \to \infty$ it is expected that the ratios tend to zero since no fluctuations are triggered. We point out that what is important for the present analysis is that E_s^r is computed at a fixed small scale whereas E_s accounts for the contribution of all of the scales. In figure 10(*a*) the ratio E_s/E_{tot} calculated for the two test cases, grid and jet, is shown on a log-log scale. A collapse of the curves is achieved at any t_i indicating that, when the total contribution of structures is considered, no difference is observed for different Re_λ. The ratios E_s^r/E_{tot}^r are reported in figure 10(*b*). In this case the agreement is observed only for $t_i \leqslant 1$, which corresponds to the non-intermittent region previously described. It is shown that the energy contribution of intermittent small-scale structures is significantly affected by the flow conditions. This gives a first indication that structures in grid and jet turbulence may have different natures since their energy is distributed over the scales in a different manner. Specifically, on the basis of previous observations (Camussi & Guj 1997), it might be assumed that jet structures involve a larger number of scales since they appear as large-scale structures. The different nature of structures in the different flow conditions will be further established in the following section. As a final remark, we point out that for high t_i (e.g. $t_i > 10$) the energy of the most intermittent structures is always lower than 10 %, in agreement with previous numerical observations on the energy contributions of vortex filaments in homogeneous isotropic turbulence (e.g. Jimenez *et al.* 1993).

5.3. *Waiting times*

The waiting times between successive events are calculated by fixing a threshold t_i and calculating the difference between consecutive time instants corresponding to $l(r, x) \geqslant t_i$. This procedure has been described in § 3 and more details may be found in Abry *et al.* (1994). Hereafter, δt denotes the random variable representing the waiting times and $\langle \delta t \rangle$ its mean value. In figure 11 the PDF of the waiting times calculated for $Re_\lambda \simeq 10$ and $Re_\lambda \simeq 800$, normalized with respect to $\langle \delta t \rangle$, are reported. The linear trend in the semi-log scale observed for $Re_\lambda \simeq 10$ corresponds to an exponential functional form which is observed for time instants larger than a time scale δt_{c1} also shown in the figure. According to previous results, the exponential decay is characterized by a coefficient $\simeq 0.5$ (see e.g. Villermaux *et al.* 1995). Furthermore, as will be shown later, when such a curve is plotted on a log-log scale (figure 12), the few points corresponding to $\delta t < \delta t_{c1}$ seem to follow a linear trend that corresponds to a power law form of the PDF in this range. As pointed out above (see also Abry *et al.* 1994), the transition from a power law to an exponential law of the waiting time PDF is an indicator of the achievement of statistical independence of the detected events. Indeed, the exponential PDF corresponds to a Poisson law which characterizes random variables which must be statistically independent.

In general, we may define as δt_c the delay time where such transition happens. For the present analysis, δt_{c1} and δt_{c2} refer respectively to the grid and jet cases. The presence of a transition for $\delta t = \delta t_c$ physically indicates that the characteristic time scale of the turbulent structures which are associated to the educed events should be of the order of, or smaller than, δt_c. At $Re_\lambda \simeq 10$, the time delay δt_{c1} corresponds, in terms of space length (see grid case of table 1), to a scale of the order of 2–3η. Therefore, we can argue that the characteristic size of the coherent structures in grid turbulence at $Re_\lambda \simeq 10$ is of the order of a few Kolmogorov lengths η and so they are dissipative since their size belongs to the dissipation range of the energy

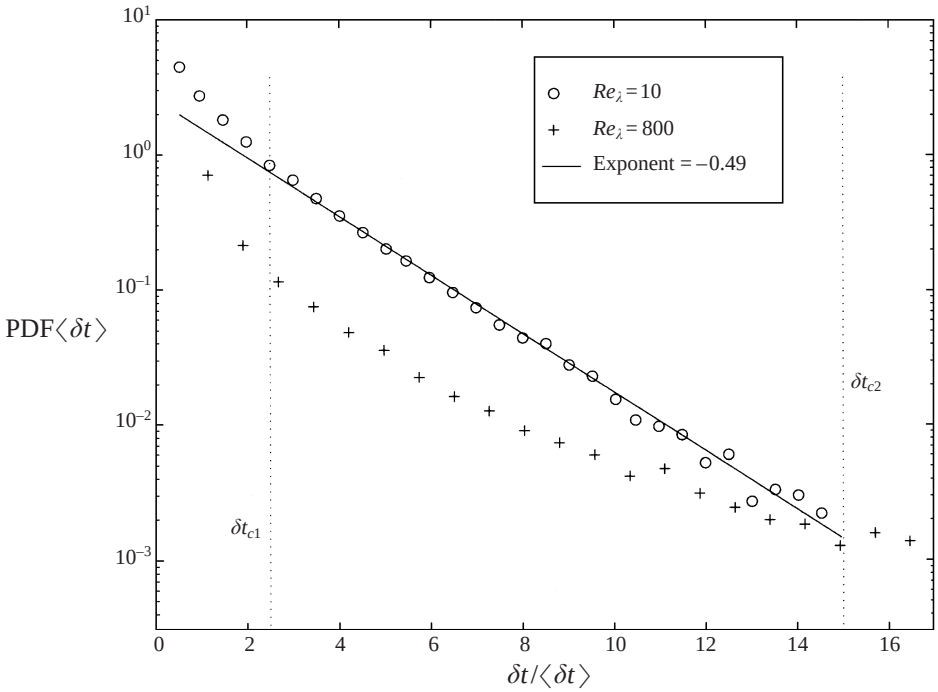

FIGURE 11. Log-linear plot of the waiting times PDF normalized with respect to $\langle \delta t \rangle$. Different symbols corresponds to different Re_λ. δt_c represents the time delay corresponding to a transition from a power to an exponential law for $Re_\lambda \simeq 10$ (δt_{c1}) or $Re_\lambda \simeq 800$ (δt_{c2}). The solid line represents the exponential fit of the points $\delta t \geqslant \delta t_{c1}$ for $Re_\lambda \simeq 10$.

spectra. However, as pointed out in Gledzer *et al.* (1996), this does not mean that the dissipation rate ϵ reaches its maximum inside such structures.

The waiting time estimation and the corresponding PDF analysis in the case of jet turbulence and $Re_\lambda \simeq 800$ are also shown in figure 11. In this case it is evident that no linear trend is observed and that the functional form is different from that observed for $Re_\lambda \simeq 10$. In figure 12, the curves of figure 11 are reported in a log-log scale. It is evident that for $Re_\lambda \simeq 10$ there is no linearity apart from a few points corresponding to very low energy fluctuations (in the range $\delta t \leqslant \delta t_{c1}$). On the other hand, for $Re_\lambda \simeq 800$, the trend is almost linear indicating that the functional form can be assumed to be a power law. As pointed out above, a power law of the waiting time PDF suggests that no statistical independence of the selected events has been achieved. We point out again that when a power law is observed for $\delta t < \delta t_c$, we may presume the characteristic (spatial) dimension of the structure to be of the order of, or less than, $\overline{V}\delta t_c$. For the case of $Re_\lambda \simeq 800$, the high turbulent dynamics spoils the accuracy of the PDF tail. However, the largest reliable time delay reported in figure 12 corresponds, in terms of space length, to a scale on the order of $\sim 100\,\eta$, that is clearly outside the dissipation range, and a transition to the exponential decay is not clearly observed. Larger delays are not reported due to the poor statistics. It is evident that, in the case of jet turbulence, it is not possible to estimate the exact value of δt_{c2}. However, it may surely be argued that the scale corresponding to δt_{c2} should not be lower than the scale corresponding to the maximum δt where a power law is observed, i.e. $\sim 100\,\eta$. Denoting by δt_{dj} and δt_{dg} the time scales corresponding to the

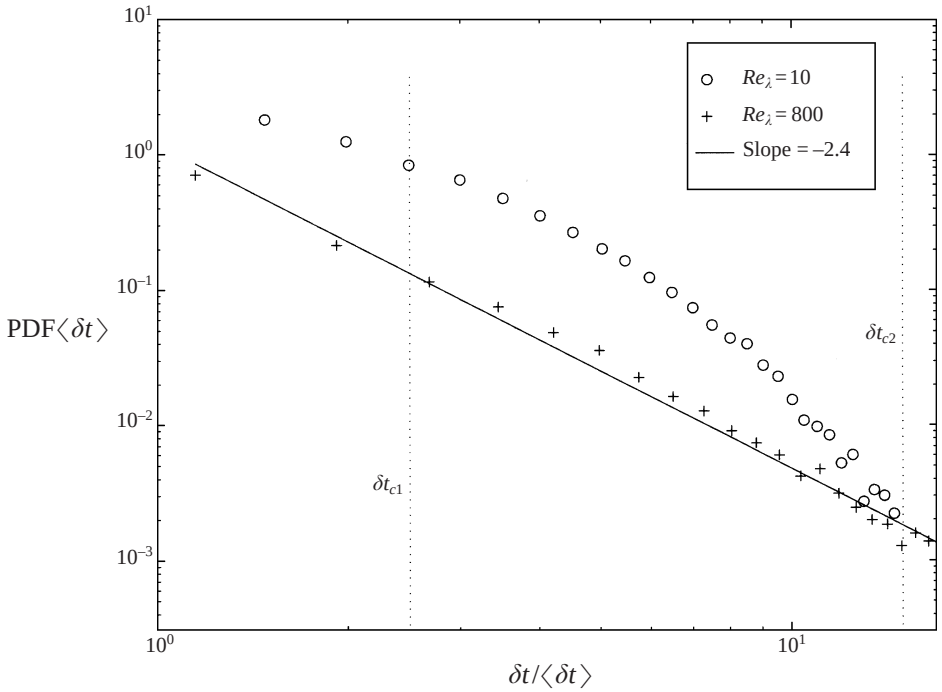

FIGURE 12. Same as figure 11 but in a log-linear scale. The solid line represents the power law fit of the points $\delta t \leqslant \delta t_{c2}$ for $Re_\lambda \simeq 800$.

dissipative lengths respectively of the jet and the grid case, it is therefore obtained that

$$\delta t_{c2}/\delta t_{dj} \simeq 100 \gg \delta t_{c1}/\delta t_{dg} \simeq 3,$$

demonstrating that the typical transition times δt_c are not universal. We finally point out that waiting time normalized PDFs are independent of the threshold t. In figure 13, an example of the normalized PDFs achieved for $t = 1, 3$ and 10 at $Re_\lambda \simeq 800$ is given. The collapse of the curves is quite satisfactory indicating that the use of different thresholds does not affect the physical meaning but may be useful to improve the statistical accuracy.

In conclusion, analysis of the waiting time statistics allows us to state that in the case of high Re_λ and jet turbulence, the characteristic size (in terms of η) of the coherent structures associated with the energy bursts is much larger than that of the structures observed in the case of low Re_λ and grid turbulence. Actually, since the analysis is performed only on one velocity component, such a conclusion refers to the longitudinal length scale of the structures or, if the Taylor hypothesis is not considered, to their typical time scale. Anyway, results presented in Camussi & Guj (1997) support the idea that the observed non-universality is due to the different types of coherent structure which characterize grid and jet turbulence.

We finally point out that, from the experimental viewpoint, such conclusions may be achieved either by directly visualizing the coherent structures (such as in Villermaux *et al.* 1995) or by suitably conditioning the anemometric data, as in the present case by the wavelet based procedure.

Once the PDFs of the waiting times are available, we can easily estimate the mean

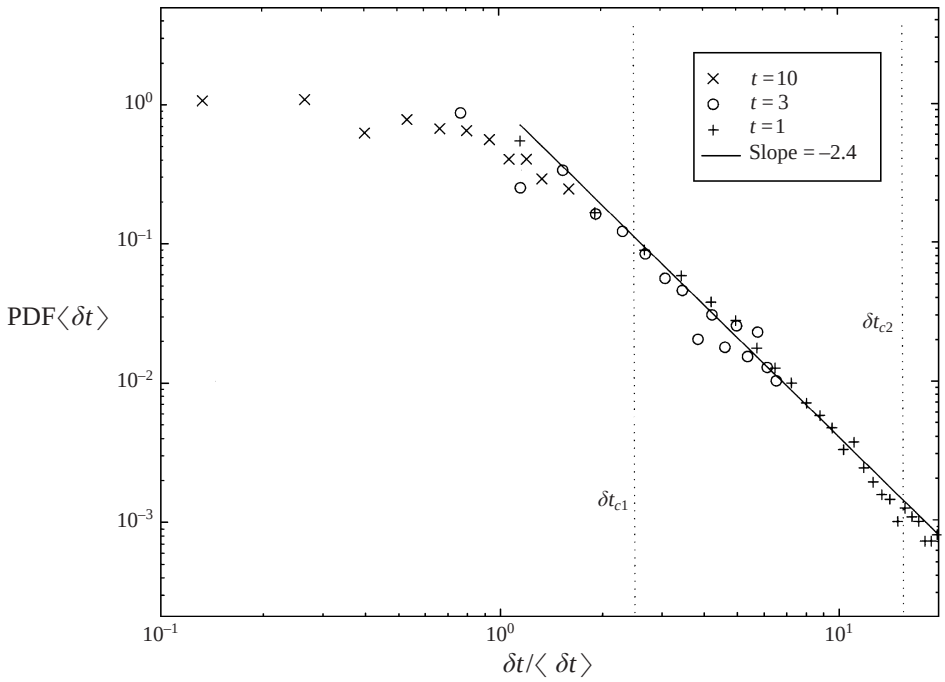

FIGURE 13. Log-log plot of the waiting times PDF for $Re_\lambda \simeq 800$. Different symbols correspond to different trigger levels ($t = 1,\ 3$ and 10).

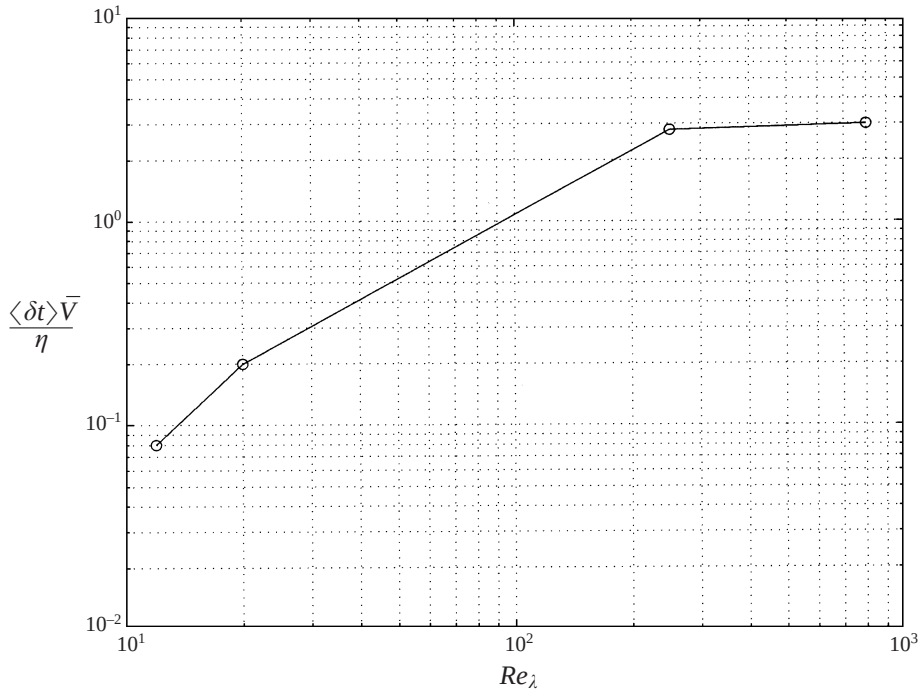

FIGURE 14. Log-log plot of the mean waiting time normalized with respect to $\eta/\overline{V}$. $Re_\lambda \simeq 20$ and $Re_\lambda \simeq 250$ correspond to other flow conditions available to the authors at intermediate Re_λ from Camussi & Guj (1997).

waiting time and normalize it with respect to a suitable time scale characteristic of the flow considered. The mean waiting time is normalized with respect to the smallest eddy turnover time available in the turbulent flow, that is estimated by the ratio $\eta/\overline{V}$. The result is plotted in figure 14 on a log-log scale. In this figure, we show also the mean dimensionless waiting times calculated for other flow conditions at intermediate Re_λ between 10 and 800 (see Camussi & Guj 1997) to have a qualitative idea of the dependence upon Re_λ. The main result is that the mean dimensionless waiting time strongly depends upon the Reynolds number: it increases with Re_λ and seems asymptotically to reach a saturation value of about ~ 3. Such a trend is also observed when the space scale instead of the time scale is considered. What is important for the present purposes is that, again, no universality is achieved and that the mean frequency of appearance of turbulent structures depends upon Re_λ. We point out that an increasing trend of the mean dimensionless waiting times has also been reported by Abry *et al.* (1994) when pressure fluctuations were analysed. These results support the idea that the time statistics of the coherent structures, as well as their characteristic size, are not universal parameters but are strongly dependent on the way turbulence is generated and on the Reynolds number of the turbulent flow.

6. Conclusions

Experimental data at $Re_\lambda = 10$ and 800, have been analysed by means of a wavelet expansion of the velocity signals. Attention has been focused on the energy fluctuations localized in time (x) and scale (r), which are formalized by the LIM function denoted by $l(r, x)$. In the present analysis a pure statistical approach has been preferred for the analysis of energy fluctuations but the results achieved sometimes show strong differences depending on which statistical indicator is considered. Such differences are related to the different physical meaning of the indicators themselves. The principal results are summarized as follows:

(i) The PDFs of the energy fluctuations (LIM) follow an exponential law or a power law depending on whether the energy distribution is intermittent or not. This functional form seems universal, since it has been observed for scales ranging from a few Kolmogorov lengths up to the integral size, and for different flow conditions. Specifically, the PDFs in the non-intermittent region, corresponding to $l(r, x) < 1$, are characterized by a power law with a scaling exponent of about -1.7 whereas the exponential law is achieved for $l(r, x) > 1$. Incidentally, the power law region of the energy PDFs is characterized by an exponent close to the $-5/3$ value expected for the inertial range of the energy spectra at high Re_λ.

(ii) The energy bursts represented by the peaks in the $l(r, x)$ distribution seem to be the only events responsible for the intermittent behaviour of the velocity structure function scaling relations usually observed in homogeneous and isotropic turbulence. As a matter of fact, when such events are eliminated in a suitable manner, the intermittency anomalies of the scaling exponents of the moments of the wavelet coefficients disappear, and the Kolmogorov scaling is achieved.

(iii) When we consider the way energy cascades from large to small scales, which is the mechanism responsible for the self-similarity which leads the velocity structure functions scaling laws (Monin & Yaglom 1975), the behaviour seems to be universal and does not depend upon Re_λ or the turbulence generator, at least for $Re_\lambda \geqslant 10$.

(iv) The characteristic size of the structures responsible for intermittency is dependent upon Re_λ and the turbulence generators, but not upon the threshold level itself.

The different size of the structures is shown by the shape of the waiting times PDFs. Therefore, the preservation of the scaling laws is only a form of apparent universality. Indeed, the coherent structures responsible for the universal scaling laws are far from universal themselves, but are strongly dependent on the turbulent flow considered.

In conclusion the present analysis supports the idea that, in agreement with previous analysis (Camussi & Guj 1997), the usually observed universal behaviour of the statistics of V_r may be induced by turbulent structures of different natures and sizes depending on the turbulent generator and on Re_λ. Indeed, we think that for a certain turbulence generator, structures are wholly responsible for the observed dynamical behaviour which may vary only if the generator itself is changed and is not dependent upon which energy fluctuation level is selected. Points (iii) and (iv) may be reconciled by the idea that the presence of intermittency is due to structures of different shape and topology depending on the turbulence generator and Re_λ. On the other hand, the way the energy is transferred from large to small scales and then dissipated seems to be universal and preserved at surprisingly low Re_λ. The present results support the idea that the energy transfer mechanism from large to small scales is universal (at least for locally homogeneous turbulent flows) and that small- and large-amplitude events are strictly correlated. From this viewpoint, the present results seem to support the validity of an infinite hierarchical structure of energy dissipation, following the theoretical model proposed by She & Levesque (1994). Indeed, according to the recent numerical results by Borotav & Pelz (1997), the observation that structures of different natures (e.g. filaments and ring vortices) lead to the same scaling exponents $\zeta(p)$ is compatible with the She & Levesque (1994) model, when the adjustable parameters are suitably chosen.

P. Abry is sincerely acknowledged for his useful suggestions and advice on the methodologies adopted for the data analysis. S. Ciliberto and C. Baudet are gratefully acknowledged for their help during the measurements performed at the ENS de Lyon (the high Re_λ case of the present work). The present research has been supported by MURST of Italy (40 % and 60 %).

REFERENCES

Abry, P., Fauve, S., Flandrin, P. & Laroche, C. 1994 Analysis of pressure fluctuations in swirling turbulent flows. *J. Phys.* (*Paris*) II **4**, 725–733.

Anselmet, F., Gagne, Y., Hopfinger, E. J. & Antonia, R. A. 1984 High-order velocity structure functions in turbulent shear flows. *J. Fluid Mech.* **140**, 63–89.

Arneodo, A., Baudet, C. & Belin, F. 1996 Structure functions in turbulence, in various flow configurations, at Reynolds number between 30 and 5000, using extended self-similarity. *Europhys. Lett.* **34**, 411–416.

Bacry, E., Arneodo, A., Frisch, U., Gagne, Y. & Hopfinger, E. 1989 Wavelet analysis of fully developed turbulence data and measurement of the scaling exponents. In *Proc. Turbulence 89: Organized Structures and Turbulence in Fluid Mechanics, Grenoble* (*France*)*, Sept. 1989* (ed. M. Lesieur & O. Metais), pp. 203–215. Kluwer.

Benzi R., Ciliberto S., Tripiccione, R., Baudet, C., Massaioli, F. & Succi, S. 1993 Extended self-similarity in turbulent flows. *Phys. Rev.* E **48**, 29–32.

Benzi, R., Ciliberto, S. & Chavarria, G. R. 1995 On the scaling of three dimensional homogeneous and isotropic turbulence. *Physica* D **80**, 385–398.

Borotav, O. N. & Pelz, R. B. 1997 Structures and structure functions in the inertial range of turbulence. *Phys. Fluids* **9**, 1400–1415.

Camussi, R. & Guj, G. 1997 Othonormal wavelet decomposition of turbulent flows: intermittency and coherent structures. *J. Fluid Mech.* **348**, 177–199.

Camussi, R. & Guj, G. 1996 Experimental analysis of scaling laws in low Re_λ grid-generated turbulence. *Exps. Fluids* **20**, 199–209.

Camussi, R., Ciliberto, S., Benzi, R. & Baudet, C. 1996*a* Statistical uncertainty in the analysis of structure functions in turbulence. *Phys. Rev.* E **54**, 100–103.

Camussi, R., Barbagallo, D., Guj, G. & Stella, F. 1996*b* Transverse and longitudinal scaling laws in anisotropic low *Re* turbulence. *Phys. Fluids* **8**, 1181–1191.

Castaing, B., Gagne, Y. & Hopfinger, E. J. 1990 Velocity probability density functions of high Reynolds number turbulence. *Physica* D **46**, 177.

Daubechies, I. 1992 *Ten Lectures on Wavelet*. CBMS-NSF Reg. Conf. Ser. Appl. Maths.

Douady, S., Couder, Y. & Brachet, M. E. 1991 Direct observation of the intermittency of intense vorticity filaments in turbulence. *Phys. Rev. Lett.* **67**, 983–986.

Dubrulle, B. 1994 Intermittency in fully developed turbulence, log-Poisson statistics and generalized scale-covariance. *Phys. Rev. Lett.* **73**, 959.

Farge M. 1992 Wavelet transforms and their applications to turbulence. *Ann. Rev. Fluid Mech.* **24**, 395–457.

Frisch, U. 1996 *Turbulence*. Cambridge University Press.

Gledzer, E., Villermaux, E., Kahalleras, H. & Gagne Y. 1996 On the log-Poisson statistics of the energy dissipation field and related problems of developed turbulence. *Phys. Fluids* **8**, 3367–3378.

Jimenez, J., Wray, A. A., Saffman, P. G. & Rogallo, R. S. 1993 The structure of intense vorticity in isotropic turbulence. *J. Fluid Mech.* **255**, 65–90.

Jorgensen, F. E. 1971 Directional sensitivity of wire and fiber-film probes. *DISA Inf. Dept.* **11**, 31–37.

Kolmogorov, A. 1941 The local structure of turbulence in incompressible viscous fluid for very large Reynolds numbers. *C. R. Akad. Sci. SSSR* **30**, 301–305.

Kuo, A. Y. S. & Corrsin, S. 1972 Experiments on the geometry of the fine-structure regions in fully turbulent fluid. *J. Fluid Mech.* **56**, 447–479.

Lundgren, T. S. 1982 Strained spiral vortex model for turbulent fine structure. *Phys. Fluids* A **25**, 2193–2203.

Lundgren, T. S. 1993 A small-scale turbulence model. *Phys. Fluids* **5**, 1472–1483.

Meneveau, C. & Sreenivasan, K. R. 1991 The multifractal nature of turbulent energy dissipation. *J. Fluid Mech.* **224**, 429–484.

Meneveau, C. 1991 Analysis of turbulence in the orthonormal wavelet representation. *J. Fluid Mech.* **232**, 469–520.

Mimouni, S., Laval, G., Scheurer, B. & Jaffard, S. 1995 Morphology of the mixing layer in the Rayleigh-Taylor instability. In *Small-Scale Structures in Three Dimensional Hydrodynamic and Magneto-hydrodynamic Turbulence* (ed. V. Meneguzzi & A. Pouquet). Lecture Notes in Physics, pp. 179–192. Springer.

Moffat, H. K. 1984 Simple topological aspects of turbulence vorticity dynamics. In *Turbulence and Chaotic Phenomena in Fluids* (ed. T. Tatsumi), pp. 223–230. North-Holland.

Monin, A. S. & Yaglom, A. M. 1975 *Statistical Fluid Mechanics*, vol. 2, MIT Press.

Pullin, D. I. & Saffman, P. G. 1992 On the Lundgren-Townsend model of turbulent fine scales. *Phys. Fluids* **5**, 126–145.

She, Z. S. & Levesque, E. 1994 Universal scaling laws in fully developed turbulence. *Phys. Rev. Lett.* **72**, 336–338.

She, Z. S. & Waymire, E. C. 1995 Quantized energy cascade and Log-Poisson statistics in fully developed turbulence. *Phys. Rev. Lett.* **74**, 262.

She, Z.-S., Jackson, E. & Orszag, S. A. 1990 Intermittent vortex structures in homogeneous isotropic turbulence. *Nature* **144**, 226–228.

Willaime, H., Belin, F., Maurer, P. & Tabeling, P. 1996 High Reynolds number experiment: transition and structures. In *Advances in Turbulence VI* (ed. S. Gavrilakis, L. Machiels & P. A. Monkewitz), pp. 271–273. Kluwer.

Tennekes, H. & Lumley, J. L. 1972 *A First Course in Turbulence*. MIT Press.

Verzicco, R., Jimenez, J. & Orlandi, P. 1995 On steady columnar vortices under local compression. *J. Fluid Mech.* **299**, 367–388.

Villermaux, E., Sixou, B. & Gagne, Y. 1995 Intense vortical structures in grid-generated turbulence. *Phys. Fluids* **7**, 2008–2013.

Vincent, A. & Meneguzzi, M. 1991 The spatial structure and statistical properties of homogeneous turbulence. *J. Fluid Mech.* **225**, 1–25.

Yamada, M., Kida, S. & Ohkitani, K. 1993 Wavelet analysis of PDFs in turbulence. In *Unstable and turbulent motion of fluids* (ed. S. Kida). World Scientific.